Radio Science, Volume 33, Number 6, Pages 1901–1913, November–December 1998

Three-dimensional nonlinear simulations of the gradient drift instability in the high-latitude ionosphere

P. N. Guzdar, N. A. Gondarenko, and P. K. Chaturvedi
Institute for Plasma Research, University of Maryland, College Park

S. Basu
Air Force Research Laboratory, Hanscom, MA

Abstract. Nonlinear three-dimensional (3-D) simulations of the gradient drift instability (GDI) are presented for a two-dimensional equilibrium density gradient representing a polar cap plasma patch. The overall evolution of structuring of the plasma patch is influenced markedly by the effects caused by dynamics parallel to the geomagnetic field. The long wavelengths ($kL_n \leq 1$) are strongly stabilized in the 3-D case, and the nonlinear state is dominated by smaller mesoscales ($kL_n \gg 1$) (where k and L_n are the mode number and density gradient scale length, respectively). The results provide an interpretation to the observations at the high-latitude ionosphere indicating a generation of mesoscale irregularities associated with the polar cap patches when the interplanetary magnetic field (IMF) B_z is southward and antisunward convection prevails over the polar cap. The polar cap patches are observed to convect to large distances (~3000 km) undergoing structuring while maintaining their distinct identity. Thus we suggest here that the inclusion of three-dimensional effects is key to a successful interpretation of high-latitude irregularities, as well as a prerequisite for a credible simulation of these processes.

1. Introduction

The ionospheric plasma at high latitudes is known to display plasma density and electric field structure which encompasses a wide range of both spatial (hundreds of kilometers to meters or less) and temporal (hours to minutes) scales [*Tsunoda,* 1988; *Kelley,* 1989; *Crowley,* 1996] (see also the special section on coupling, energetics, and dynamics of atmospheric regions, *Radio Science*, 29(1), 155-405, 1994). These irregularities have been studied using ground-based radio and optical techniques, in situ spacecraft measurements, and scintillation techniques, among others. The large or macroscales (hundreds of kilometers) are obviously of global origin and have been characterized as "patches" (in the polar cap), or "blobs" (at auroral latitudes) [*Weber et al.,* 1984, 1986; *Basu et al.,* 1990; *Basu et al.,* 1994]. The medium scales (also referred to as "mesoscale"), in the range of 0.1 km to a few kilometers, may be the result of a local process such as a plasma instability. The observations [*Weber et al.,* 1986; *Basu et al.,* 1994] and modeling studies [*Sojka et al.,* 1993] indicate that the patches convect to long distances, ~3000 km [*Weber et al.,* 1986] and for long periods of time (hours) while retaining their distinct identity.

Paper number 98RS01703.
0048-6604/98/98RS-01703$11.00

The polar cap patches in effect very much resemble a plasma cloud, as they drift from the cusp region to the polar cap (in the antisunward direction at speeds ~100-1000 m/s). Mesoscale irregularities are observed in association with these patches throughout the polar cap region [*Weber et al.,* 1984, 1986; *Tsunoda,* 1988; *Basu et al.,* 1990; *Basu et al.,* 1994], with irregularities often being more intense on the trailing edge than on the leading edge [*Weber et al.,* 1984], suggesting that the gradient drift instability (GDI) is a likely generation mechanism.

In this paper, three-dimensional (3-D) nonlinear simulations are presented for the gradient drift instability (GDI). The 3-D analytical treatments in the collisional regime for the GDI [*Drake et al.,* 1988; *Chaturvedi and Huba,* 1987] show that dynamics parallel to the geomagnetic field are stabilizing at long wavelengths. We first present numerical results of the role of the parallel electric field on the linear growth rate of the nonlocal GDI for a two-dimensional density equilibrium with variation transverse to the ambient magnetic field and variation along the field. We then present a simulation of the nonlinear evolution of the patches/blobs at late times. Numerically, a code for the nonlocal GDI, including the parallel dynamics, is developed for an equilibrium transverse density gradient profile more realistic than the ones hitherto considered, as well as one with a variation along the field line. Numer-

ical simulations show that with the inclusion of 3-D effects, nonlinear evolution is dominated by a generation of mesoscales, and the deleterious long wavelengths are suppressed. The evolution takes place on timescales comparable to observation. The extent of smaller-scale generation is determined by the ambient parameters and the characteristic parallel scale size of the system (such as the parallel size of polar cap patch/auroral blob). This presents a natural explanation of the observation of polar cap patches traveling large distances while undergoing structuring, but still retaining their identity. In the two-dimensional (2-D) fluid simulations (transverse to the ambient magnetic field) [*Mitchell et al.*, 1985] due to the lack of stabilization by parallel electron dynamics, the instability is very strong, thus breaking up the original patch into smaller patches in a very short period of time, less than an hour.

2. Equations for the Gradient Drift Instability

The starting equations are the continuity and momentum transfer equations for electrons and ions, and, the current-conservation equation. The derivation of equations describing the GDI with parallel effects is as follows. For the GDI modes the primary motion across the magnetic field is the $\mathbf{E} \times \mathbf{B}$ drift, and the inclusion of parallel dynamics introduces the resistive electron motion. The current conservation equation, also known as the "potential" or "vorticity" equation, has contributions from differential collisional motion between ions and electrons in a direction across the magnetic field and from the parallel resistive electron motion. The two coupled equations, for a collisional plasma in a uniform magnetic field along the z direction, describing these modes are thus the electron continuity equation and the vorticity equation [*Drake et al.*, 1988],

$$\frac{\partial n}{\partial t} - \frac{c}{B_0}\nabla\phi \times \hat{z} \cdot \nabla n + \frac{\partial}{\partial z}\frac{1}{e\eta_e}\left[\frac{\partial \phi}{\partial z} - \frac{T_e}{ne}\frac{\partial n}{\partial z}\right] = 0. \tag{1}$$

$$\frac{c}{B_0}\frac{\nu_{in}}{\Omega_i}\nabla_\perp \cdot (n\nabla_\perp \phi) + \frac{\nu_{in}}{\Omega_i}\left(\hat{z} \times \vec{V_n}\right) \cdot \nabla n + D_{\perp i}\nabla_\perp^2 n + \frac{\partial}{\partial z}\frac{1}{e\eta_e}\left[\frac{\partial \phi}{\partial z} - \frac{T_e}{en}\frac{\partial n}{\partial z}\right] = 0. \tag{2}$$

where most of the symbols have their standard meanings: n, c, e, ϕ, T, and $\vec{V_n}$ refer to plasma density, velocity of light, electronic charge, electrostatic potential, temperature in energy units, and the neutral wind velocity, respectively. Furthermore, $D_{\perp i} = \nu_{in} c T_i/\Omega_i e B_0$, $D_\parallel = T_e/m_e\nu_e$, $\eta_e = m_e\nu_e/ne^2$, and $\Omega_a = e_a B_0/m_a c$ ($e_a = \pm e$) is the cyclotron frequency of species $\alpha(e, i)$. Also, $\nu_e = \nu_{ei} + \nu_{en}$ is the sum of the electron-ion and electron-neutral collision frequencies, and ν_{in} is the ion-neutral collision frequency. In the above set, ion inertia effects have not been included. For the coordinate system representing the high-latitude ionosphere, Earth's field lines are nearly vertical and assumed aligned with the z axis, the x axis points southward, and the y axis is in the west-east direction. In the frame of reference of the patch, the flow velocity is in the x direction. As a consequence in the stationary Earth frame, the patch moves in the negative x direction, which is the northward direction. Thus the left side of the patch with the positive density gradient is the leading edge, and the right side of the patch with the negative density gradient is the trailing edge. A set of typical parameters at the high-latitude ionosphere is $T_e \approx T_i \approx 0.1$ eV; $L_n \approx 50$ km; $V_n \approx 500$ m/s; $\gamma_0 = V_n/L_n \approx 10^{-2}\ s^{-1}$; $\Omega_e \approx 10^7$ rad/s; $\Omega_i \approx 10^2$ rad/s; $\nu_{ei} \approx 5 \times 10^3\ s^{-1}$; and $\nu_{in} \sim 0.1\ s^{-1}$.

Next, we discuss some well-known limits of the linear gradient drift instability from the above set of equations, with special attention to the effects of parallel dynamics and its application to polar cap patch/auroral blob. In the mesoscale size limit, we can do a simple local linear theory analysis by assuming all the perturbed quantities to be of the form $\exp(\gamma t + ik_z z + ik_y y)$. The growth rate for the gradient drift instability (GDI) with finite k_z is [*Chaturvedi and Huba*, 1987]

$$\gamma = -\frac{k_y^2}{k_y^2 + k_z^2\left(\frac{\Omega_e\Omega_i}{\nu_e\nu_{in}}\right)}\frac{1}{n_0}\frac{dn_0}{dx}V_n. \tag{3}$$

Here n_0 is the equilibrium density. The neutral wind flow velocity was assumed to be in the positive x direction. The above expression shows that finite k_z has a strong stabilizing influence, especially for $k_y^2 \ll k_z^2\Omega_e\Omega_i/\nu_e\nu_{in}$. This is so because of the large value of the factor $(\Omega_e\Omega_i/\nu_e\nu_{in}) = 10^6$-$10^8$ in the F region. Thus long wavelengths satisfying $\lambda_\perp > 2\left(\Omega_e\Omega_i/\nu_e\nu_{in}\right)^{1/2}$ are strongly stabilized. Here L_z is the characteristic scale size of the patch/blob in the parallel direction, 500-1000 km. However, for a realistic equilibrium, which has variations along the field, the choice of k_z is not arbitrary and is deter-

mined by the natural variation of the equilibrium density. Therefore in the next section we first investigate, using a two-dimensional linearized code, the linear growth and the three-dimensional mode structure of these modes. This is then followed by a fully nonlinear three-dimensional simulation of the GDI instability.

3. Numerical Results

We rewrite the set (1)-(2) in their dimensionless form as

$$\frac{\partial n}{\partial t} - \frac{L_n}{L_0}\nabla\phi \times \hat{z} \cdot \nabla n = D_\perp \nabla_\perp^2 n + D_\parallel \nabla_\parallel^2 n. \quad (4)$$

$$\nabla \cdot (n\nabla\phi) + \frac{\partial n}{\partial y} = 0. \quad (5)$$

$$\nabla = e_x\partial_x + e_y\partial_y + (\beta)^{1/2} e_z \partial_z \quad (6)$$

where the following normalizations have been used: $t \rightarrow t(V_n/L_n)$, $\phi \rightarrow \phi(c/L_0 V_n B_0)$, $n \rightarrow n/N_0$, $z \rightarrow z/L_z$, $x \rightarrow x/L_0$, and, where L_0 is the patch scale length, N_0 is the undisturbed ambient density of the background ionosphere away from patch/blob (independent of x); and the dimensionless parameter β is

$$\beta = \frac{\Omega_e \Omega_i}{\nu_e \nu_{in}} \frac{L_0^2}{L_z^2}. \quad (7)$$

In Figure 1a we display the computation box. The size of the box in the x, y directions transverse to the direction z of the geomagnetic field is 8π, whereas the size of the box along z is 4π. In Figure 1b, the variation of the density profile in the x direction is shown. The density gradually decreases to the ambient levels, away from the patch/blob boundary. This is clearly a fairly realistic representation of the density gradient likely to exist at the trailing edge of a convecting polar cap patch. Previous work on the gradient drift instability for 3-D perturbations, accounting for the parallel dynamics, considered either a simple exponential gradient [*Chaturvedi and Huba*, 1987] or the "water-bag" model (which was applied to plasma cloud studies) [*Drake et al.*, 1988]. The variation of the density profile along the direction of the geomagnetic field (z axis) is shown in Figure 1c. In the absence of any dissipation, this is a true equilibrium. In the presence of the small dissipation, this profile changes very slowly due to diffusion on the timescale of the instability and the nonlinear structuring. Therefore, even in the presence of dissipation, the given profile can be viewed as a equilibrium based on the timescale arguments. Thus our two-dimensional patch model is an improvement on the previous analyses of the GDI, especially in its application to the high-latitude environment consisting of polar cap patches/auroral blobs.

To clearly show the effect of the third dimension along the field lines, we first compute the linearized growth rates and typical mode structure for the GDI modes obtained by linearizing the system of equations (4) and (5). A 2-D finite difference time-dependent code has been developed to numerically solve the linearized equations. The number of grid points in x and z are N_x=101 and N_z=51. An initial perturbation, $\tilde{n} = 0.001 \sin(2\pi m y/L_y)\sin(\pi x/L_x)$, was introduced, with m the mode number in the y direction. The diffusion coefficients chosen for these runs are $D_\perp$=10^{-5} and $D_\parallel$=10^{-5}. The boundary conditions used for the perturbed density and potential are the following. In the x direction, $\phi(0, y, z) = \phi(L_x, y, z) = n(0, y, z) = n(L_x, y, z) = 0$. For the boundary conditions in the z direction we choose the Neumann conditions for both the perturbed density and the potential. In Figure 2a we show the growth rate as a function of the mode number m for β=0, 10, 50, and 500. What is clearly seen is the reduction of the growth rate as the parameter β is increased. The reduction in the growth rate occurs preferentially for the lower values of m. The numerically computed growth rates for the fully nonlocal case are in qualitative agreement with the local theory growth given in equation (3). However, for this nonlocal case both the k_x and k_z are determined by the variation in the equilibrium density profile. Also, since this is a time-dependent code, it is the fastest-growing eigenmode for a given m that the code converges to. In Figure 2b we show the isosurface for the eigenmode for m=5 and β=200. The mode has localized on the unstable density gradient side of the plasma patch. Along the geomagnetic field (z direction), there is a finite localization of the mode. The initial perturbation did not have any variation along the field line. The structure developed along the field line in the region of the patch where the instability growth is the strongest. This natural creation of parallel electric field in the patch is responsible for the reduction of the growth rates. The parallel electric field tries to short out the transverse electric field caused by the instability, thereby reducing the growth rate. Also, since the fastest-growing modes are obtained

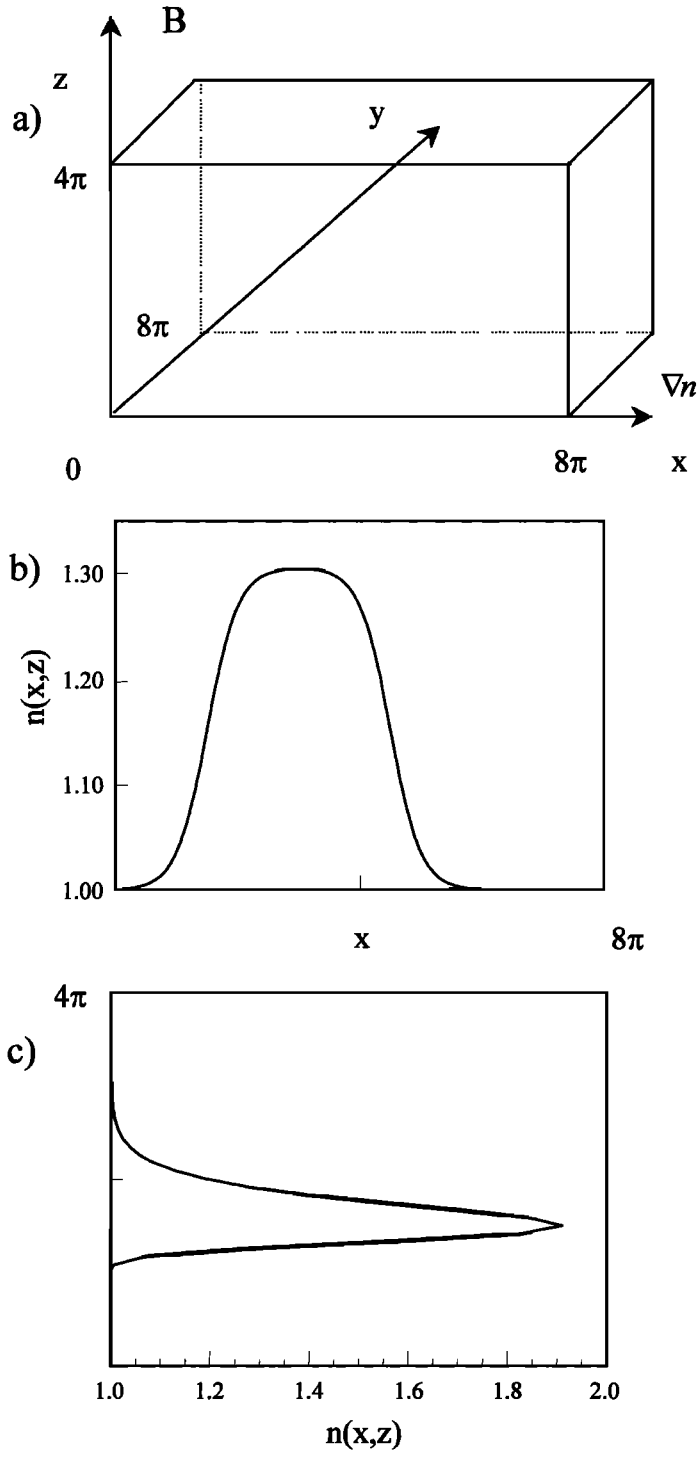

Figure 1. (a) Geometry and size of the three-dimension computation box; (b) equilibrium density profile in the x direction; and (c) equilibrium density profile in the z direction.

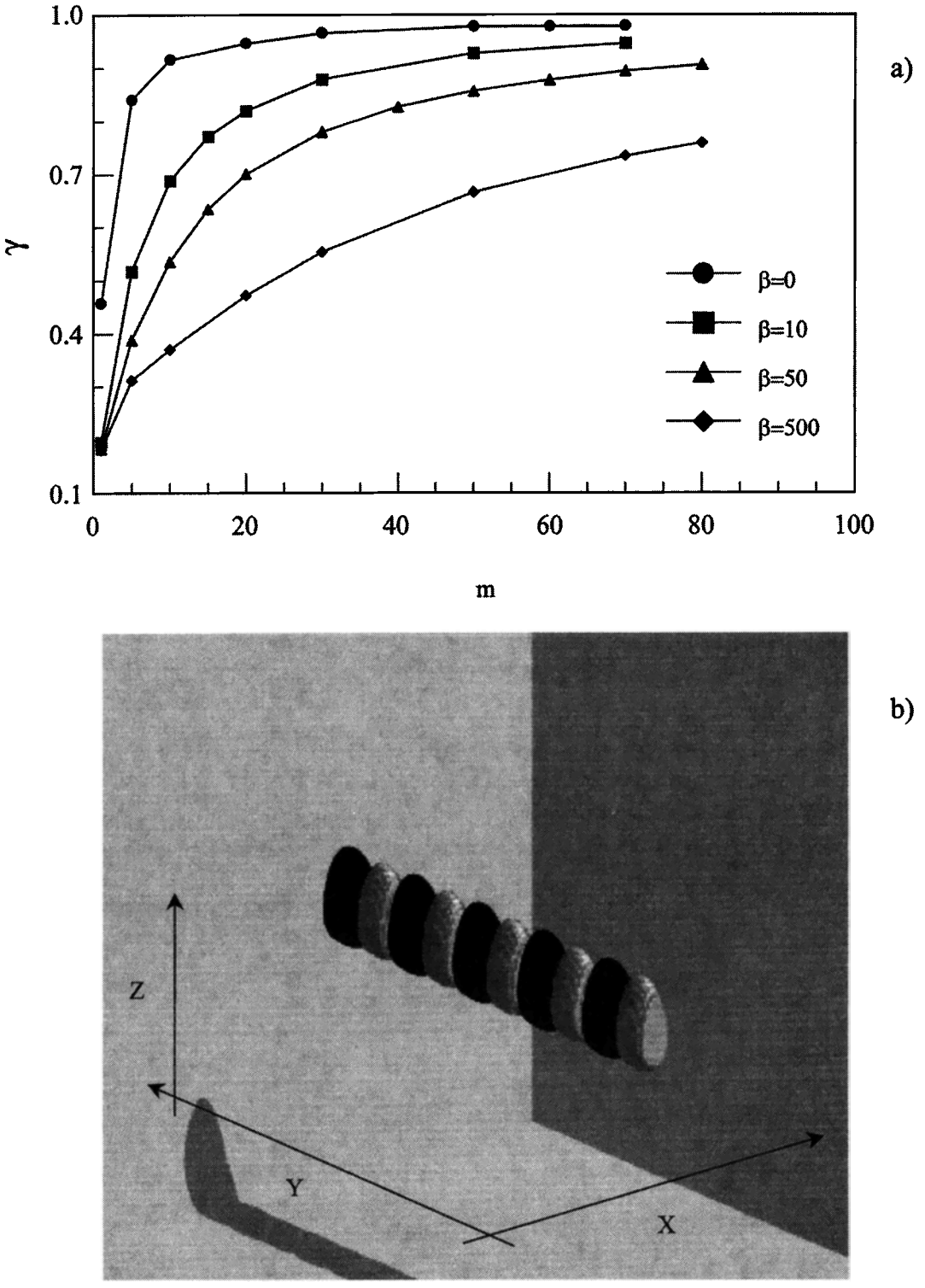

Figure 2. (a) Growth rate as a function of mode number m for β=0, 10, 50, and 500, and (b) isosurface of the potential for m=5, β=200, and $D_{\perp}=D_{||}=10^{-5}$.

with the time-dependent code, it is also clear that the lowest mode number in the x direction as well as the z direction is the most unstable. This is consistent with the local growth rate in equation (3), which shows that the smallest values of k_x and k_z give the largest growth for a given k_y. Thus we have demonstrated that the inclusion of the dynamics along the field leads to significant reduction of the growth rates for the gradient drift instability in plasmas patches and as a consequence must be included to shed light on the observed structuring of the patches. Another important consequence of this study is that there a natural parallel electric field that develops due to the gradient drift instability.

We now proceed to the solution of the system of nonlinear equations (4) and (5). A fully nonlinear three-dimensional finite difference code has been developed to solve these coupled equations. As shown in Figure 1 for a characteristic scale length of L_0 of 20 km, the size of the computation box in the x, and y directions is 160π km. In the z direction we choose L_z=1000 km. We use a value of the parameter β=200. Typically, larger values of β would be more realistic for the bigger patches. However, due to available computer resources, this choice of β is reasonable and would be valid for the smaller-sized patches. The transverse diffusion $D_\perp=2\times10^{-3}$. Once again, as in the case of the linearized system of equations,we use the Dirichlet boundary conditions for the perturbed density and potential at x=0 and L_x. Similarly, in the z direction we use the Neumann boundary conditions at z=0 and $z=L_z$ for the perturbed density and potential. We initialize the perturbed density as a superposition of m=1-70 sine modes in the y direction with random phases. The variation in the x direction is $\sin(\pi x/L_x)$ for each of the modes. Finally, as in the linear case, we do not introduce any variations for the initial perturbations in the z direction. The amplitude of each of the harmonics is assumed to be inversely proportional to the transverse wavenumber of the mode. The number of grid points used in these simluations are N_x=101, N_y=260, and N_z=51. The initial amplitude multiplier for each of the modes was assumed to be 0.001. For this set of parameters, the normalized timescale t_0=200 s for a wind velocity of 100 m/s.

In Figures 3a-3d we show the evolution of the density in the xy plane near the peak of the density profile in z, at four different instants of time, t=8, 24, 40, and 66. As in the linear case, the instability grows on the unstable side of the density gradient. In the early nonlinear phase (t=8), the modes develop. However, they are not large enough in amplitude to modify the ambient density gradient. The structuring is dominated at the short wavelengths in the y direction. As time progresses, the modes grow to large enough amplitude to modify the original density, and the structuring leads to the formation of very fine scaled fingers penetrating the bulk of the density gradient. This is clearly seen at the times t=24 and 40. Finally, at t=66, the fingers have penetrated to the stable side of the density gradient. What is clearly seen is that there is a significant extention of the average density gradient on the unstable side of the original density gradient, while the original density gradient on the left side, is not that significantly modified. This is consistent with some of the observations [*Basu et al.*, 1990], which show a strong asymmetry in the gradient scale lengths between the leading and trailing edges of the patch. In terms of the real time this corresponds to approximately 4 hours. We hasten to add that the absolute timescale should not be taken as final since it depends on the dissipation used in our code. What really matters is the relative timescale for two different values of β. In a second run we used β=10. For this case the structuring is very similar in spatial character to the β=200 case. This is to be expected since in both the cases the shorter wavelengths are the fastest growing, as shown in Figure 2a. However, the structuring occurred on a much faster timescale. It reached the level of structuring shown in Figure 3d in about one third the time. In earlier two-dimensional simulations by *Mitchell et al.* [1985], the patch had disintegrated into smaller-sized patches in less than an hour due to the severity of the instability in two dimensions. In Figures 4a-4d we display the potential contours at the same instants of time as the density in Figure 3. Since the equilibrium potential is zero for the chosen 2-D density equilibrium, even at t=8, the potential perturbation localized on the unstable gradient is clearly seen. With the passage of time one sees the rapid expansion of the structure along the x direction as the fingers penetrate into the bulk of the plasma patch. The rapid acceleration of the fingering process in the nonlinear phase can be understood as follows. As the perturbation develops, very steep localized density gradients develop in the fingers. Since the growth rate of the instability is inversely proportional to the density gradient scale length L_n, the fingering proceeds faster. However, we

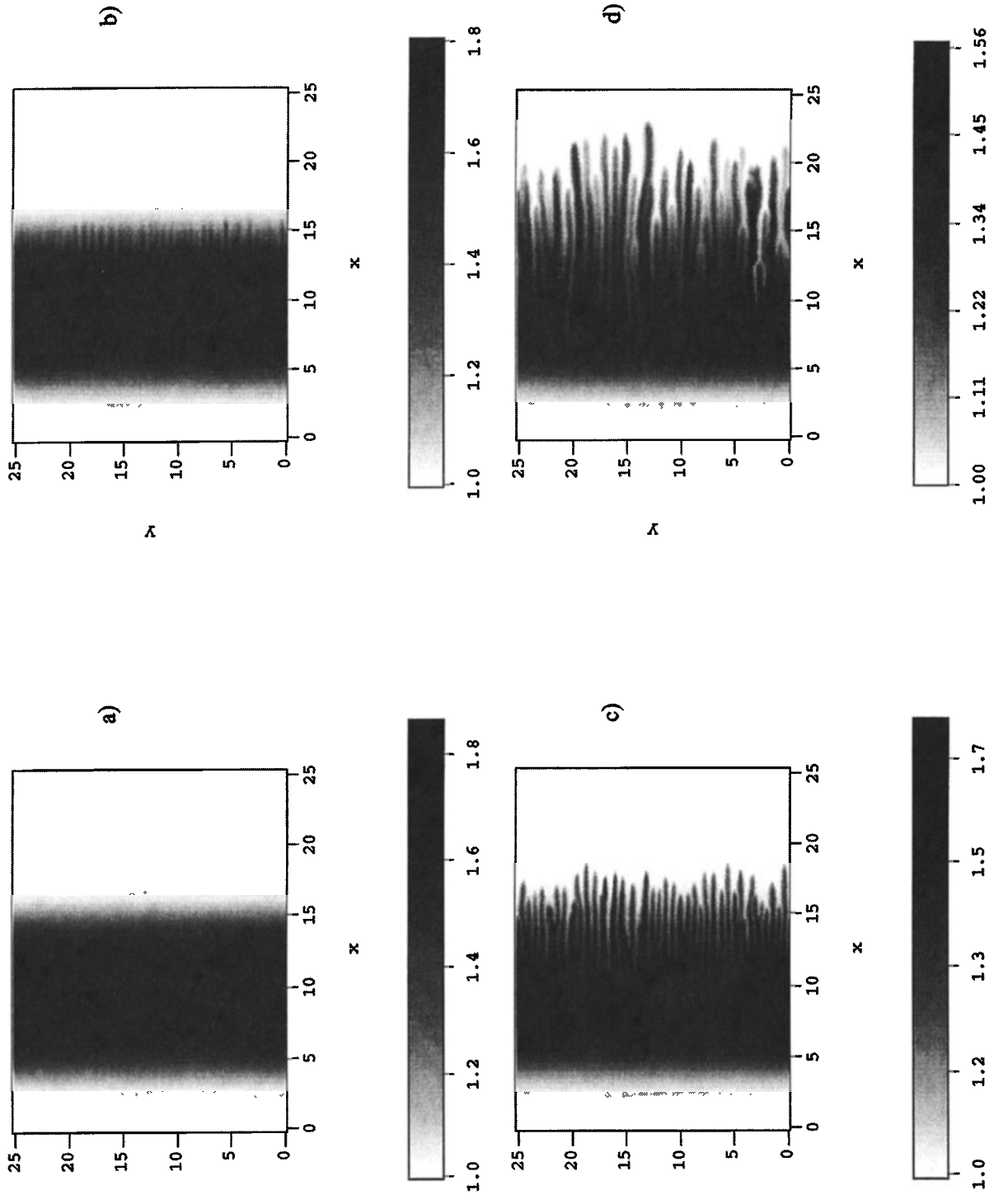

Figure 3. Density contours in the xy plane at $z=L_z/4$ for (a) $t=8$, (b) $t=24$, (c) $t=40$, and (d) $t=66$. The parameters used are $\beta=200$ and $D_\perp=D_\parallel=2\times10^{-3}$.

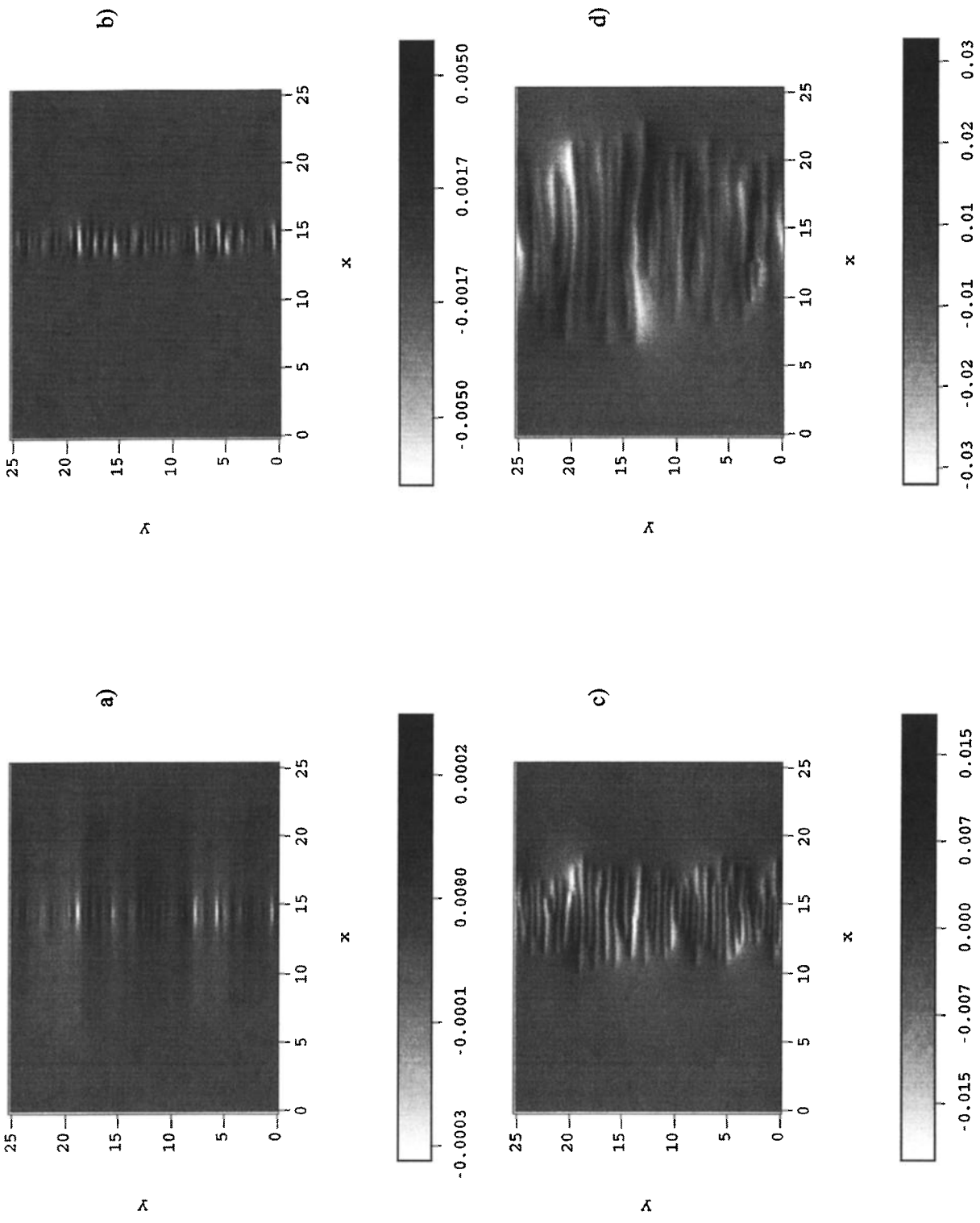

Figure 4. Potential contours in the xy plane at $z=L_z/4$ for (a) $t=8$, (b) $t=24$, (c) $t=40$, and (d) $t=66$. The parameters used are $\beta=200$ and $D_\perp=D_\parallel=2\times10^{-3}$.

have found that as we go to higher β, the timescale for the process increases because of the stabilizing influence of large β, as seen in the linear studies (Figure 2a). In Figures 5a-5d and 6a-6d we show the density and potential contours in the xz plane at t=8, 24, 40, and 66. What is seen is that in the very early phase the localization of the potential in the z direction is very strong. This is also consistent with our linear studies which show this feature (Figure 2b). At later times we find that there is some nonlinear spreading of the structure of the potential along the field lines.

One of the most interesting aspects of the simulations is the generation of parallel electric fields along the field line due to the gradient drift instability. The potential has been normalized to $L_0V_nB_0/c$. This can be viewed as an upper bound on the potential drop along the field lines. For L_0=20 km and V_n=100 m/s, this corresponds to about 100 V. In our simulations the maximum potential is about 0.05-0.1 of this maximum value. Thus these potentials can have interesting consequences on both the precipitating electrons [*Rosenberg et al.*, 1993] and the ionospheric oxygen ions in the high-latitude ionosphere. The ions can be accelerated out of the lower ionosphere from the peak of the potential in the F region, to heights where other transverse heating mechanisms can efficiently accelerate them to much larger energies and into the magnetosphere. Low-energy precipitating electrons can be deflected by the potential, thereby reducing the number density of precipitating electrons during the occurrence of plasma patches. This will be investigated more thoroughly in the future by using the field-aligned potential obtained from the code and studying the dynamics of test particles (electrons) precipitating along the field line or the dynamics of test oxygen ions distributed along the field line in accordance with a hydrostatic equilibrium model.

Finally, in Figure 7 we show the density as a function of x, y at z=$L_z/4$. The ambient density gradient on the trailing edge is shallower than the density gradient on the leading edge. The structuring process is like an anomalous diffusion which causes an asymmetry in the plasma patch gradients.

4. Discussion

We have presented both linear two-dimensional and nonlinear three-dimensional (3-D) simulations of the gradient drift instability (GDI), applicable to the high-latitude plasma density enhancements (polar cap patches/auroral blobs), with a realistic density gradient profile. There is compelling evidence of structuring associated with the gradients in the data [*Tsunoda*, 1988; *Basu et al.*, 1990]. However, the existing theories and simulations have not been able to explain the fact that the observed fluctuation scale lengths approximately kilometers are significantly shorter than the ambient density gradient scale length (~20 km) [*Basu et al.*, 1990]. In addition, the polar cap patches appear to traverse large distances (~3000 km) [*Weber et al.*, 1986], involving long timescales approximately hours [*Sojka et al.*, 1993; *Basu et al.*, 1995], retaining their identity even though the scintillation measurements suggest that all along they were undergoing mesoscale structuring. This implies that the generation of mesoscale structure by the GDI on the walls of patches/blobs is limited so as not to destroy the integrity of the parent patch (blob). Linear theories of the 2-D $\mathbf{E} \times \mathbf{B}$ instability do indicate that shorter wavelengths are more unstable than the longer wavelengths comparable to the density gradient scale lengths [see, e.g., *Guzdar et al.*, 1982, Figure 1a]. However, 2-D nonlinear simulations [*Mitchell et al.*, 1985] indicate that at late times the longer wavelengths dominate and break up the plasma into smaller blobs. *Tsunoda* [1988] has suggested the possibility of "freezing" scales in the high-latitude observations (roughly between hundreds of meters to a few kilometers), in analogy with observations of freezing scales in the artificial plasma clouds released in the ionosphere. We have clearly demonstrated by analytic arguments and have verified by numerical simulations that the 3-D effects cause a stabilization of the long wavelengths. The short scale sizes are stable due to diffusion. The observed density gradient scale length on the unstable side of the patches/blob (trailing edge) is found to be longer than the scale length of the blob on the stable side [*Basu et al.*, 1990]. This suggests that the presence of the small-scale density fluctuations manifests itself as anomalous particle transport, which leads to a preferential flattening of the density gradient on the unstable side. This aspect of observations has been clearly reproduced in our simulations (Figure 7).

The present study is only a first step in modeling the structuring of polar cap patches. Clearly, there is a need to build more realistic models of the patch as well as to introduce more physics into the model for the structuring. One undesireable feature

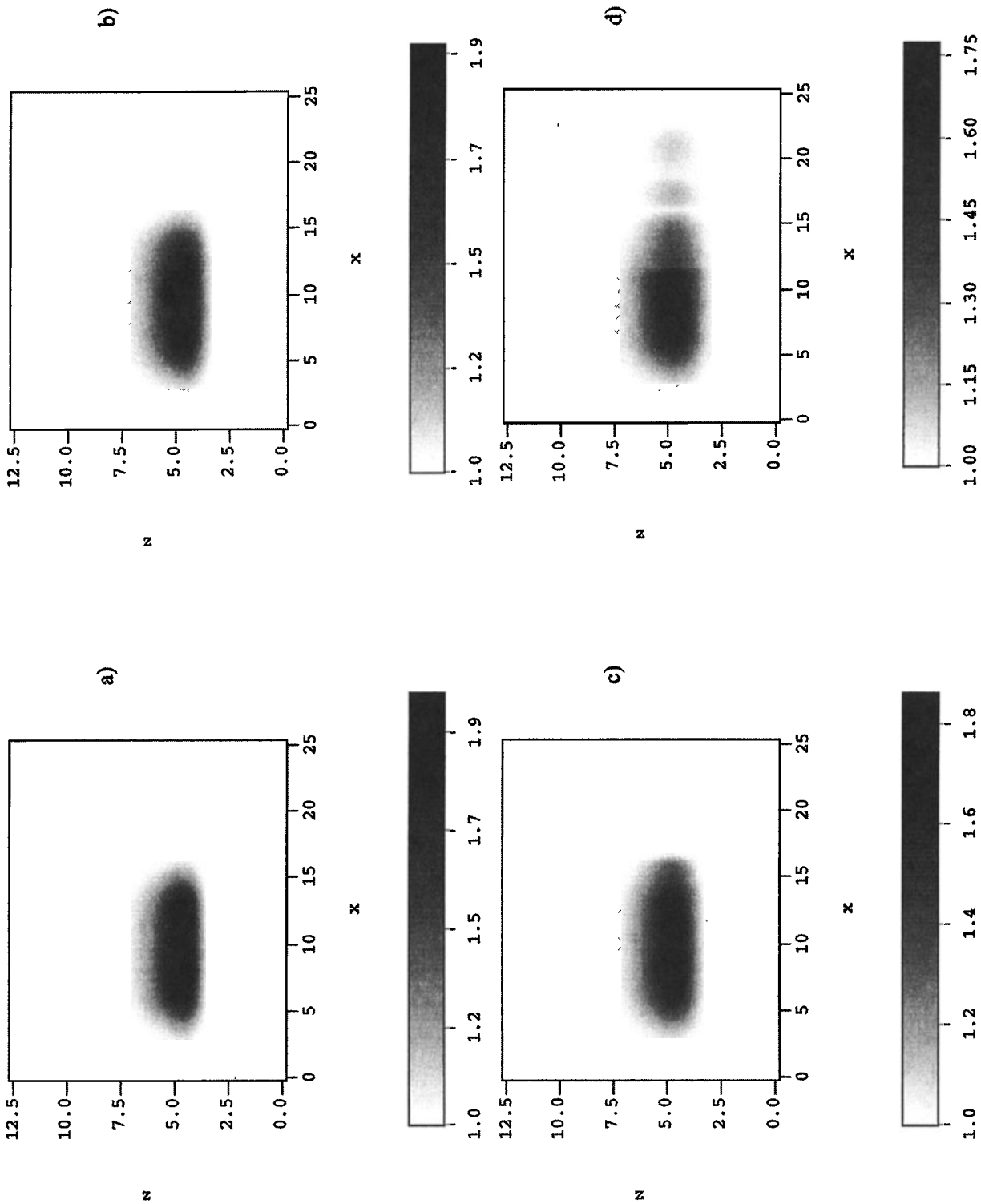

Figure 5. Density contours in the xz plane at $y=L_y/2$ for (a) t=8, (b) t=24, (c) t=40, and (d) t=66. The parameters used are β=200 and $D_\perp = D_{||} = 2 \times 10^{-3}$.

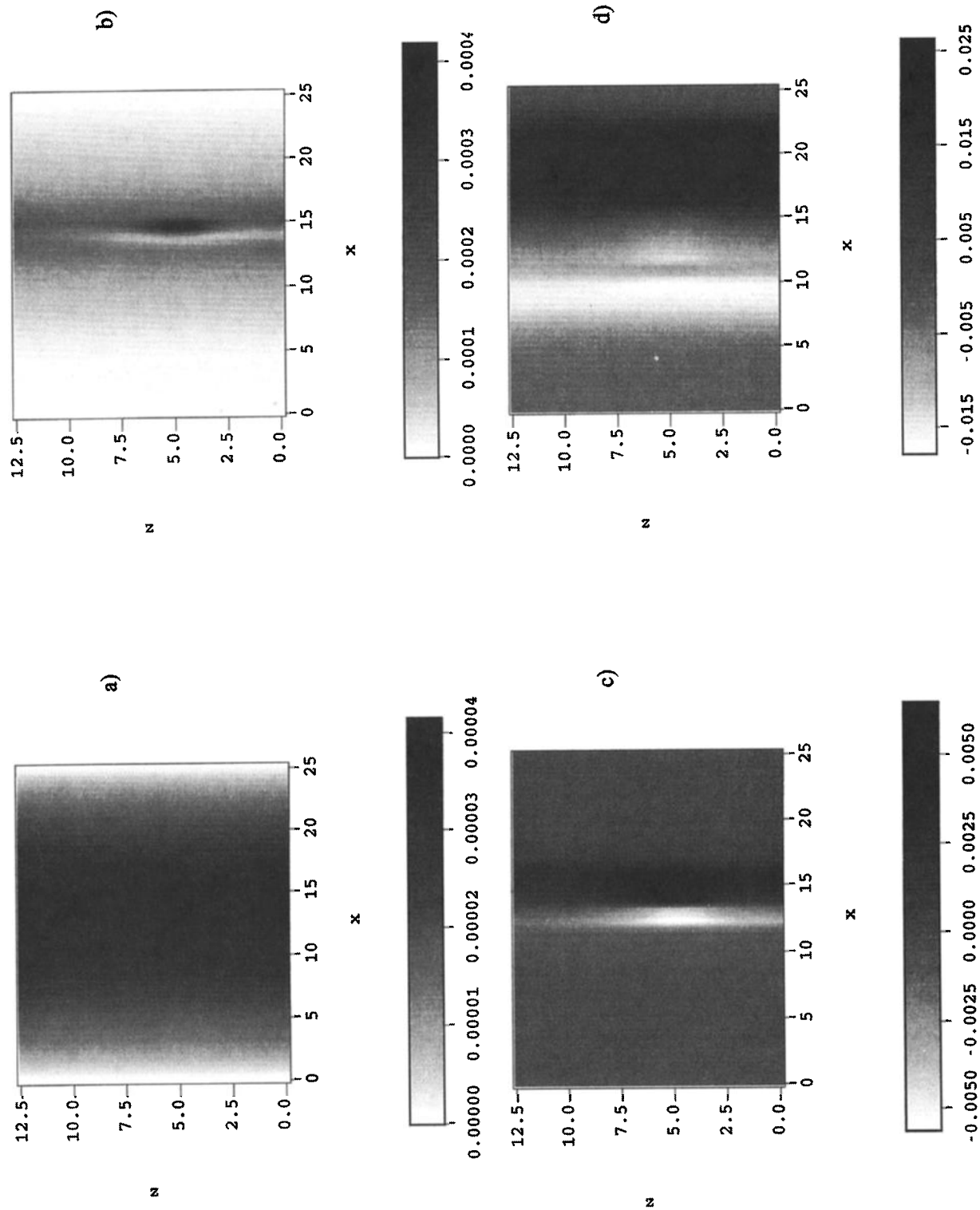

Figure 6. Potential contours in the xz plane at $y=L_y/2$ for (a) $t=8$, (b) $t=24$, (c) $t=40$, and (d) $t=66$. The parameters used are $\beta=200$ and $D_\perp=D_\parallel=2\times10^{-3}$.

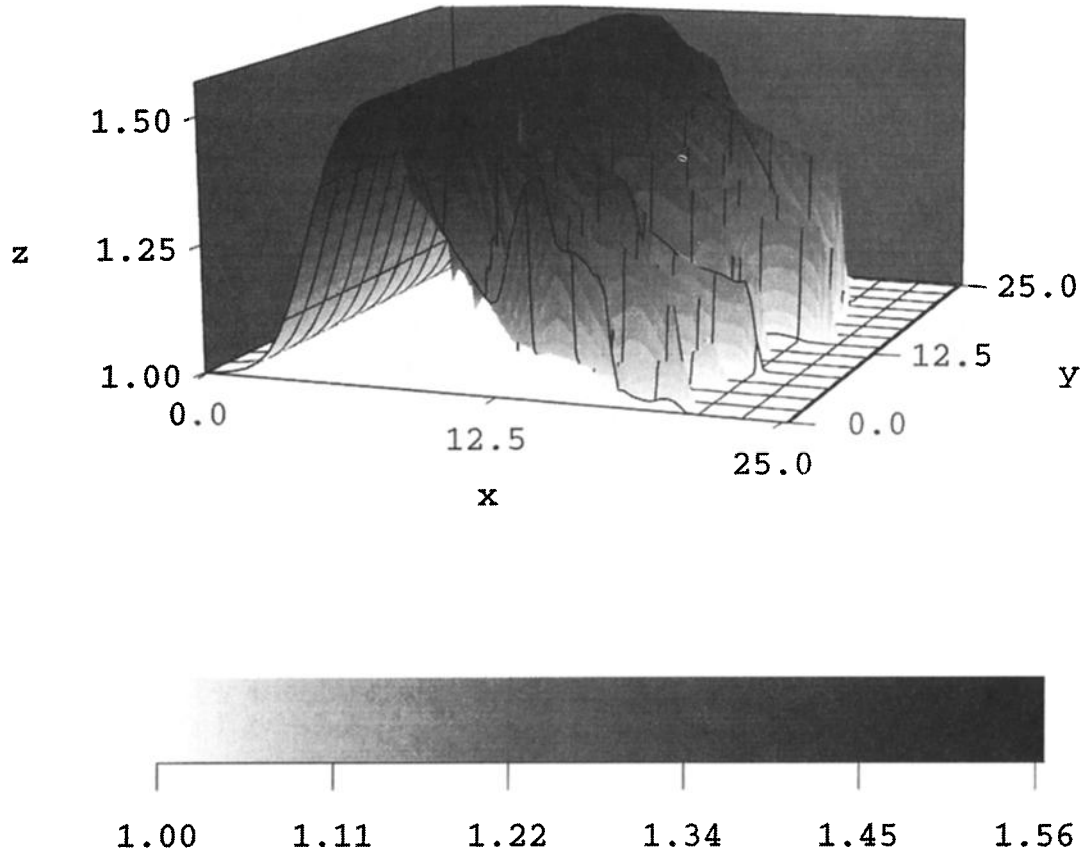

Figure 7. Density in the xy plane at $z=L_z/4$ for t=66. The parameters used are β=200 and $D_\perp=D_{||}=2\times10^{-3}$.

of our simulations is the dependence of the small-scale structure size and timescale of structuring on the diffusion used in the code. This can be remedied by introducing ion inertial effects as discussed below. Another unrealistic aspect of the present simulations is the amplitude and asymmetry of the x and y structures of the density irregularities. Although the structuring with our 3-D model shows that the very short scales dominate, it is important to realize that the simulated elongated fingers are not consistent with observations. There is no clear evidence of such strong asymmetry in the x and y directions in the fluctuation spectrum. Also, the large levels of density fluctuations of the order of 100% are not consistent with the observations, where density flucutations are more in the range of 10% (R. Heelis et al., private communication, 1997). One important physics aspect that has been neglected in these simulations is the role of the linear and the nonlinear inertial effects. For the short wavelength modes these are important since the nonlinear inertial effects can lead to breakup of the fingers, thereby removing the strong asymmetry. Furthermore, the breakup of the fingers will invariably prevent fluctuation levels as high as those obtained in our present simulations. Also, it is quite possible that the breakup scale length rather than dissipation will determine the shortest scale lengths allowed. Another important consideration is the fact that as the polar cap patch moves antisunward, there is a distortion of the patch as well as a time-dependence to the flow velocity, both of which can influence the evolution of the development of the gradient drift instability and the subsequent structuring. These issues will be the systematically addressed in future studies.

Acknowledgments. We acknowledge useful discussions with Sunanda Basu. This research was sup-

ported by the NSF under grant ATM-9416078. The work at Phillips Laboratory was partially supported by AFOSR under task 2310G9.

References

Basu, S., Su. Basu, P. K. Chaturvedi, and C. M. Bryant Jr., Irregularity structures in the cusp/cleft and polar cap regions, *Radio Sci.*, 29, 195, 1994.

Basu, S., Su. Basu, J. J. Sojka, R. W. Schunk, and E. MacKenzie, Macroscale modeling and mesoscale observations of plasma density structures in the polar cap, *Geophys. Res. Lett.*, 22, 881, 1995.

Basu, Su., S. Basu, E. MacKenzie, W. R. Coley, J. R. Sharber, and W. R. Hoegy, Plasma structuring by the gradient drift instability at high latitudes and comparison with velocity shear driven processes, *J. Geophys. Res.*, 95, 7799, 1990.

Chaturvedi, P. K., and J. D. Huba, The interchange instability in high-latitude plasma blobs, *J. Geophys. Res.*, 92, 3357, 1987.

Crowley, G., Critical Review on Ionospheric Patches and Blobs, *The Review of Radio Sci.*, Oxford University Press, 1, 1996.

Drake, J. F., M. Mulbrandon, and J. D. Huba, Three-dimensional equilibrium and stability of ionospheric plasma clouds, *Phys. Fluids*, 31, 3412, 1988.

Guzdar, P. N., P. Satyanarayana, J. D. Huba, and S. L. Ossakow, Influence of velocity shear on the Rayleigh-Taylor instability, *Geophys. Res. Lett.*, 9, 547, 1982.

Kelley, M. C., *The Earth's Ionosphere*, Academic, San Diego, Calif., 1989.

Mitchell, H., Jr. J. A. Fedder, M. J. Keskinen, and S. T. Zalesak, A simulation of high-latitude F layer instabilities in the presence of magneto-sphere ionosphere coupling, *Geophys. Res. Lett.*, 12, 283, 1985.

Rosenberg, T. J., Z. Wang, A. S. Rodger, J. R. Dudeney, and K. B. Baker, Imaging Riometer and HF Radar Measurements of Drifting F region Electron Density Structures in the Polar Cap, *J. Geophys. Res.*, 98, 7757, 1993.

Sojka, J. J., M. D. Bowline, R. W. Schunk, D. T. Decker, C. E. Valladares, R. Sheehan, D. N. Anderson, and R. A. Heelis, Modeling polar cap F region patches using time varying convection, *Geophys. Res. Lett.*, 20, 1783, 1993.

Tsunoda, R. T., High-latitude F region irregularities: A review and synthesis, *Rev. Geophys.*, 26, 719, 1988.

Weber, E. J., J. Buchau, J. G. Moore, J. R. Sharber, R. C. Livingston, J. D. Winningham, and B, W. Reinisch, F layer ionization patches in the polar cap, *J. Geophys. Res.*, 89, 1683, 1984.

Weber, E. J., J. A. Klobuchar, J. Buchau, H. C. Carlson Jr., R. C. Livingston, O. de la Beaujardiere, M. McCready, J. G. Moore, and G. J. Bishop, Polar cap F layer patches: Structure and dynamics, *J. Geophys. Res.*, 91, 12121, 1986.

S. Basu, Air Force Research Laboratory, 29 Randolph Road, Hanscom, MA 01731. (e-mail: santimay@aol.com)

P. K. Chaturvedi, N. A. Gondarenko, and P. N. Guzdar, Institute for Plasma Research, University of Maryland, College Park, MD 20742. (e-mail: guzdar@ipr.umd.edu)

(Received January 19, 1998; revised May 8, 1998; accepted May 20, 1998.)